Enhanced Antibacterial Performance of PANI–CdS/Au Nanocomposites Synthesized by Chemical Routes

Raad Al-Kilabi , Abdulameer H. Ali , Hude Al-Allaq , Elias F. Muhammed , Sahib Alkulaibi , Adel Alkhayatt , Haider Al-Hello *

Posted Date: 27 February 2026

doi: 10.20944/preprints202602.1192.v1

Keywords: gold nanoparticles; polyaniline; nanocomposites; UV–Vis; FTIR; XRD; antibacterial activity; CdS

 doi:10.20944/preprints202602.1192.v1

Article

Enhanced Antibacterial Performance of PANI–CdS/Au Nanocomposites Synthesized by Chemical Routes

Raad Al-Kilabi [1], Abdulameer H. Ali [1], Hude Al-Allaq [1], Elias F. Muhammed [2], Sahib Alkulaibi [1], Adel Alkhayatt [3] and Haider Al-Hello [2,*]

[1] College of Education for Women, University of Kufa, Najaf 54001, Iraq
[2] Faculty of Dentistry, University of Cordoba, Najaf 54001, Iraq
[3] College of Medicine, University of Alkafeel, Najaf 54001, Iraq
* Correspondence: haider.h.aziz@nust.edu.iq; Tel.: +9647883507776

Abstract

Polyaniline-cadmium sulfide-gold (PANI-CdS-Au) nanocomposites were synthesized with varying Au loadings (0.023, 0.046, 0.092)wt% to enhance antibacterial performance. Structural (FTIR, XRD) and morphological (FE-SEM) analyses confirmed successful formation, strong interactions among components, and homogeneous nanoparticle dispersion. UV–Vis spectra revealed gold surface plasmon resonance and polaronic transitions consistent with PANI emeraldine base. XRD results showed the expected wurtzite CdS and fcc Au phases. Agar well diffusion tests against Escherichia coli (Gram-negative) and Staphylococcus aureus (Gram-positive) demonstrated that the 0.092 wt% of Au composite produced the largest inhibition zones at 100 μg mL^{-1} (E. coli: 36 mm; S. aureus: 24 mm), with the same trend at 25 μg mL^{-1}. These results position PANI-CdS-Au nanocomposites as promising antibacterial materials; additional cytotoxicity assays are recommended for biomedical translation.

Keywords: gold nanoparticles; polyaniline; nanocomposites; UV–Vis; FTIR; XRD; antibacterial activity; CdS

1. Introduction

Polyaniline (PANI) is a versatile conductive polymer widely used in sensors, photocatalysis, and electrochemical applications due to its excellent electrical conductivity and reducing properties [1]. Numerous studies have investigated low-dimensional PANI structures and their organic–inorganic nanocomposites [2,3]. Among the various synthesis methods, interfacial polymerization is considered a simple and cost-effective approach for producing low-dimensional PANI [4,5].

Noble metal-based PANI nanocomposites exhibit enhanced optical and electrical properties, attributed to surface plasmon resonance and the free-electron characteristics of metallic nanostructures [6,7]. For biomedical applications, gold nanoparticles typically outperform other inorganic nanoparticles due to their superior biocompatibility with human cells [8,9], ease of production [10,11], facile bioconjugation with a variety of molecules (including polyethylene glycol (PEG), carboxyl groups, amines, DNA, RNA, antibodies, and peptides) [12,13], chemical stability [14], and adaptable engineering [15,16].

It is well established that cadmium (Cd) has no biological role and is hazardous to humans [17]. The antioxidant defense system may be impaired by reactive oxygen species (ROS) generated through oxidative stress caused by Cd bioaccumulation in human tissues, leading to various health problems [18]. In contrast, cadmium sulfide (CdS) is a luminescent material with superior optical and electrical properties, photocatalytic activity, and reduced toxicity compared to Cd, making it useful in medical applications [19,20]. CdS nanoparticles (NPs) can be synthesized through physical,

 doi:10.20944/preprints202602.1192.v1

chemical, and biological processes. Their applications depend on features such as size, shape, and surface charge, which are determined by the synthesis method [21].

Biologically synthesized CdS NPs are increasingly used in medical sciences due to their enhanced compatibility with biological systems and reduced toxicity [22]. Their non-toxicity, combined with antioxidant, antimicrobial, anticancer, imaging, and drug delivery properties, has made CdS NPs valuable as therapeutic and diagnostic tools in both in vitro and in vivo models [23,24].

In this study, a PANI–CdS/Au nanocomposite was prepared. PANI was synthesized via chemical polymerization using aniline as the monomer and ammonium persulfate (APS) as the oxidizing agent. CdS nanoparticles were subsequently synthesized using the sol–gel technique. Gold nanoparticles were produced by reduction, with varying amounts incorporated to form the PANI–CdS/Au composite. The resulting materials were characterized using UV–Vis spectroscopy, Fourier-transform infrared spectroscopy (FTIR), X-ray diffraction (XRD), and field emission scanning electron microscopy (FESEM). The antibacterial activity of the nanocomposite was evaluated using the agar well diffusion method.

2. Materials and Methods

2.1. Synthesis of AuNPs

The Gold nanoparticles were prepared by reducing hydrated gold(III) chloride ($HAuCl_4 \cdot 3H_2O$, 99%, HIMEDIA) using sodium citrate ($Na_3C_6H_5O_7$) as the reducing agent. One gram of $HAuCl_4 \cdot 3H_2O$ was dissolved in 200 mL of deionized water in a 500 mL volumetric flask to obtain a crude solution with a concentration of 14.7 mM. This solution was then diluted to 250 mL to achieve the desired concentration and stored in a brown bottle to prevent photodegradation.

Simultaneously, 0.5 g of $Na_3C_6H_5O_7$ was dissolved in 50 mL of deionized water to prepare a 1% (38 mM) sodium citrate solution. To avoid contamination, all glassware was thoroughly rinsed and cleaned with purified water prior to synthesis.

For nanoparticle preparation, 3 mL of the 1% sodium citrate solution was diluted with 250 mL of distilled water in a 500 mL Erlenmeyer flask placed on an electric stove equipped with a stirring motor. The solution was heated to 60–70 °C under continuous stirring. Subsequently, 3 mL of the 14.7 mM gold solution was added dropwise to the rapidly stirred citrate solution. The mixture gradually turned a dark crimson color, indicating the successful formation of gold nanoparticles.

2.2. Preparation of Polyaniline (PANI) Polymer

Polyaniline (PANI) was synthesized via chemical oxidative polymerization using ammonium persulfate (APS) as the oxidizing agent and catalyst in an acidic medium. A three-neck flask was cooled to 0 °C in an ice bath, and 5 mL of aniline was dissolved in 100 mL of 1.0 M hydrochloric acid. In parallel, 50 mL of 1.0 M HCl and 15 g of APS were dissolved in a separating funnel. After 30–40 minutes of mixing, the two solutions were combined and stirred continuously for 24 hours.

Upon reaching room temperature, a dark green precipitate of polyaniline was obtained. The precipitate was filtered, washed with deionized water and methanol, and dried in an oven at 353 K for 24 hours, yielding polyaniline emeraldine salt (PANI-ES) as an agglomerated powder.

To prepare emeraldine base (PANI-EB), the PANI-ES was deprotonated with NH_4OH for 15 minutes. Oligomers were removed by washing with methanol, and the resulting PANI-EB was dried in an oven at 60 °C for 24 hours before being ground into a fine powder.

2.3. Synthesis of CdS Nanoparticles

Cadmium acetate ($Cd(CH_3COO)_2 \cdot 2H_2O$) and thiourea ($CH_4N_2S$) were used as cadmium and sulfur sources, respectively, in the sol–gel synthesis of CdS nanoparticle powder. A solution containing 3 g of cadmium acetate and 2 g of thiourea in 40 mL of methanol was vigorously stirred for 1 hour at 60 °C, producing a gel-like substance. After heating was discontinued, the mixture was

 doi:10.20944/preprints202602.1192.v1

agitated until a yellow powder formed. Monocrystalline CdS nanoparticles were obtained by drying the powder at 300 °C for 30 minutes.

2.4. Synthesis of PANI–CdS/Au Nanocomposite Powder

The e appropriate amounts of PANI and CdS were dispersed in 80 mL of deionized water. To this mixture, the required volume of Au solution and acid was added, resulting in immediate reduction. The suspension was stirred for 15 minutes for each experiment, yielding the PANI–CdS/Au nanocomposite powder.

2.5. Characterization Techniques

The crystal structure was analyzed using a Philips XRD-6000 Shimadzu powder X-ray diffraction (XRD) spectrometer. XRD patterns were recorded in the range of 10–80°, with a step width of 0.021° and a step time of 1.25 seconds, employing CuKα radiation (λ = 1.5406 Å). Fourier-transform infrared (FTIR) spectroscopy of PANI, PANI–CdS, and PANI–CdS/Au nanocomposites (0.023, 0.046, and 0.092 mg) was performed in the frequency range of 400–4000 cm^{-1} using a Shimadzu FTIR-8400S. Morphological analysis was carried out using field emission scanning electron microscopy (FESEM, Quanta 450, Czech) operating at 20 kV. UV–Vis absorption and transmission spectra of PANI, PANI–CdS, and PANI–CdS/Au nanocomposites (0.023, 0.046, and 0.092 wt%) were recorded in the wavelength range of 200–1100 nm using a MEGA-2100 UV–Vis spectrophotometer (SCINCO, Korea).

2.6. Antibacterial Activity of PANI–CdS/Au Nanocomposites

The antimicrobial activity of PANI–CdS/Au nanocomposites (0.023, 0.046, and 0.092 wt%) was evaluated against two clinical bacterial strains: Escherichia coli (Gram-negative) and Staphylococcus aureus (Gram-positive), using the agar well diffusion method. A standardized bacterial suspension (1.5×10^8 CFU/mL, 0.5 McFarland standard) was swabbed onto Mueller–Hinton agar plates using sterile cotton swabs. Wells (9 mm diameter) were created using a sterilized corn borer, and 100 µg/mL and 25 µg/mL of each nanocomposite were introduced into separate wells. Plates were incubated at 37 °C for 24 hours, after which inhibition zones were measured in millimeters.

3. Results

3.1. UV-vis Analysis

The UV–Vis absorption spectra of gold nanoparticles and PANI–CdS/Au nanocomposites exhibit pronounced optical signatures indicative of strong electronic interactions within the hybrid system (Figure 1). The gold nanoparticles display a distinct surface plasmon resonance (SPR) band centered at ~518–530 nm, a hallmark of their formation, which also accounts for the characteristic ruby-red coloration of the colloidal suspension.

For PANI in its emeraldine base (EB) form, absorption bands are observed at ~343 nm and ~759 nm, consistent with π–π^* transitions in the conjugated backbone and polaron-related transitions in the near-infrared region. These spectral features corroborate earlier reports of PANI EB, where the lower-energy band reflects the delocalization of charge carriers and their coupling with π orbitals.

Upon incorporation of CdS and Au nanoparticles into the PANI matrix, the nanocomposites exhibit enhanced absorption intensity and progressive red-shifts of the near-infrared band (754–775 nm) as the Au content increases (0.023, 0.046, and 0.092 wt%). This red-shift signifies a transition toward lower-energy photon absorption, arising from plasmonic–semiconductor–polymer coupling. The strengthening of the SPR band with higher Au loading confirms increased nanoparticle density, while the spectral evolution highlights improved charge-transfer dynamics between PANI, CdS, and Au.

At the highest Au concentration (0.092 wt%), the red-shift is most pronounced, suggesting maximized plasmonic enhancement and extended light-harvesting capability. Such behavior is particularly relevant for optoelectronic and photocatalytic applications, as the broadened absorption

 doi:10.20944/preprints202602.1192.v1

facilitates efficient electron transfer and reactive oxygen species (ROS) generation, thereby augmenting the nanocomposite's antimicrobial activity.

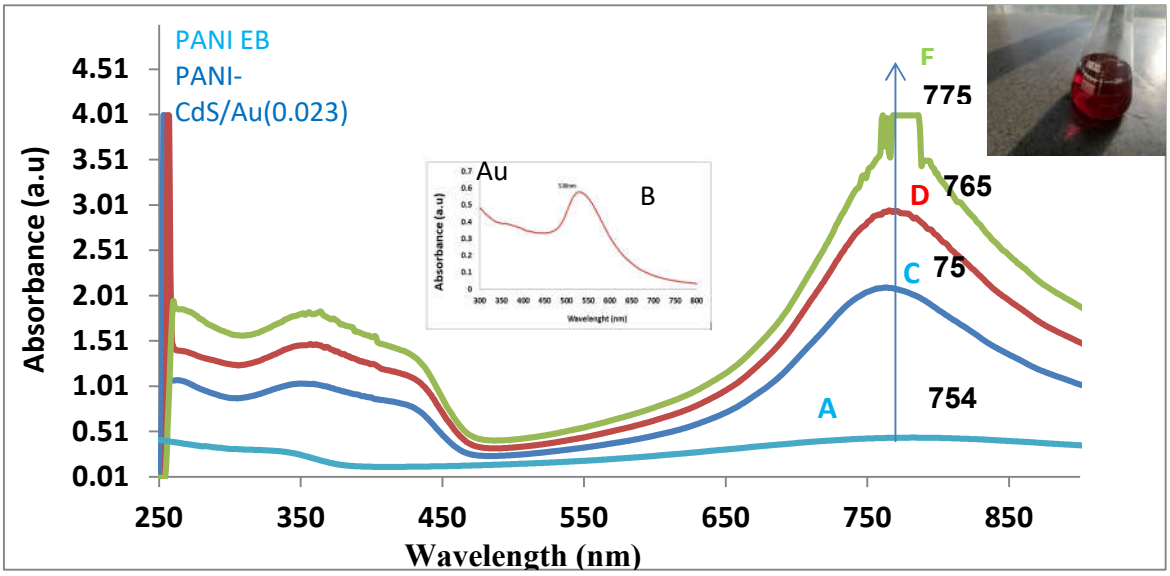

Figure 1. Absorbance spectra of (A) polyaniline (PANI) in its emeraldine base form, (B) gold nanoparticles (Au NPs), and (C–E) PANI-CdS/Au nanocomposites at different Au weight percentages: C. 0.023 wt%, D. 0.046 wt%, and E. 0.092 wt%. The spectra show characteristic absorbance peaks, with the main band observed in the range of 754–775 nm, corresponding to the nanocomposite samples. The inset (B) highlights the localized surface plasmon resonance (LSPR) peak of Au NPs around 518 nm.

3.2. Fourier Transform Infrared Analysis

This study presents Fourier-transform infrared (FTIR) spectra of pristine PANI, CdS nanoparticles, and PANI–CdS/Au nanocomposites. The FTIR spectrum of PANI exhibits characteristic absorption bands at ~1591 and ~1491 cm^{-1}, corresponding to quinoid and benzenoid ring vibrations, respectively. The band at 1381 cm^{-1} is attributed to C–N stretching of aromatic amine groups, while absorptions at 1163–1061 cm^{-1} are associated with C–N^{+} stretching in the emeraldine salt structure. The peak at ~827 cm^{-1} corresponds to out-of-plane C–H bending vibrations, confirming the emeraldine form of PANI.

The FTIR spectrum of CdS nanoparticles reveals a distinct absorption band at ~775 cm^{-1}, which is assigned to Cd–S bond stretching. Additionally, the band at ~1632 cm^{-1} corresponds to bending vibrations of adsorbed water molecules (H–O–H), while the broad absorption near 3310 cm^{-1} is indicative of hydroxyl (O–H) groups, likely arising from surface-bound species.

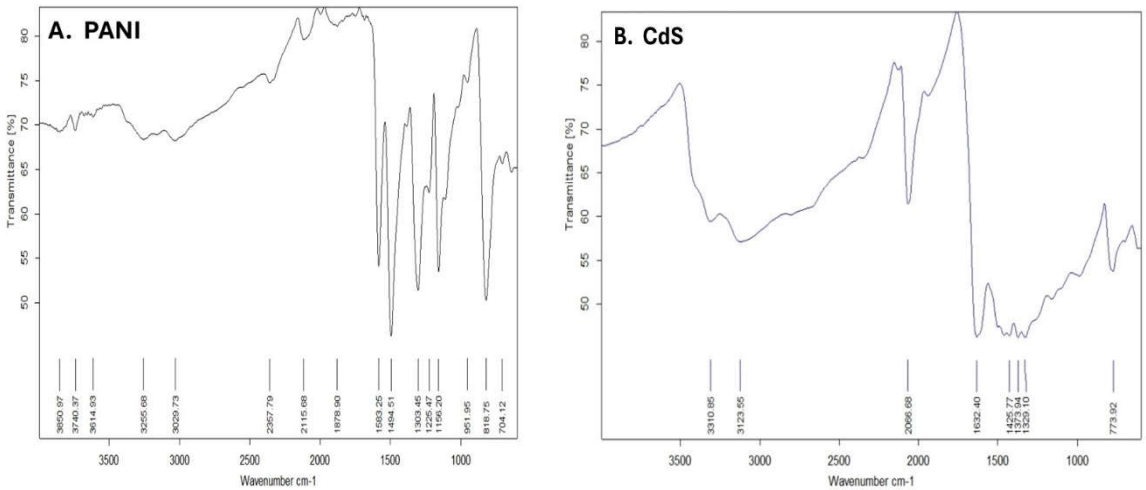

 doi:10.20944/preprints202602.1192.v1

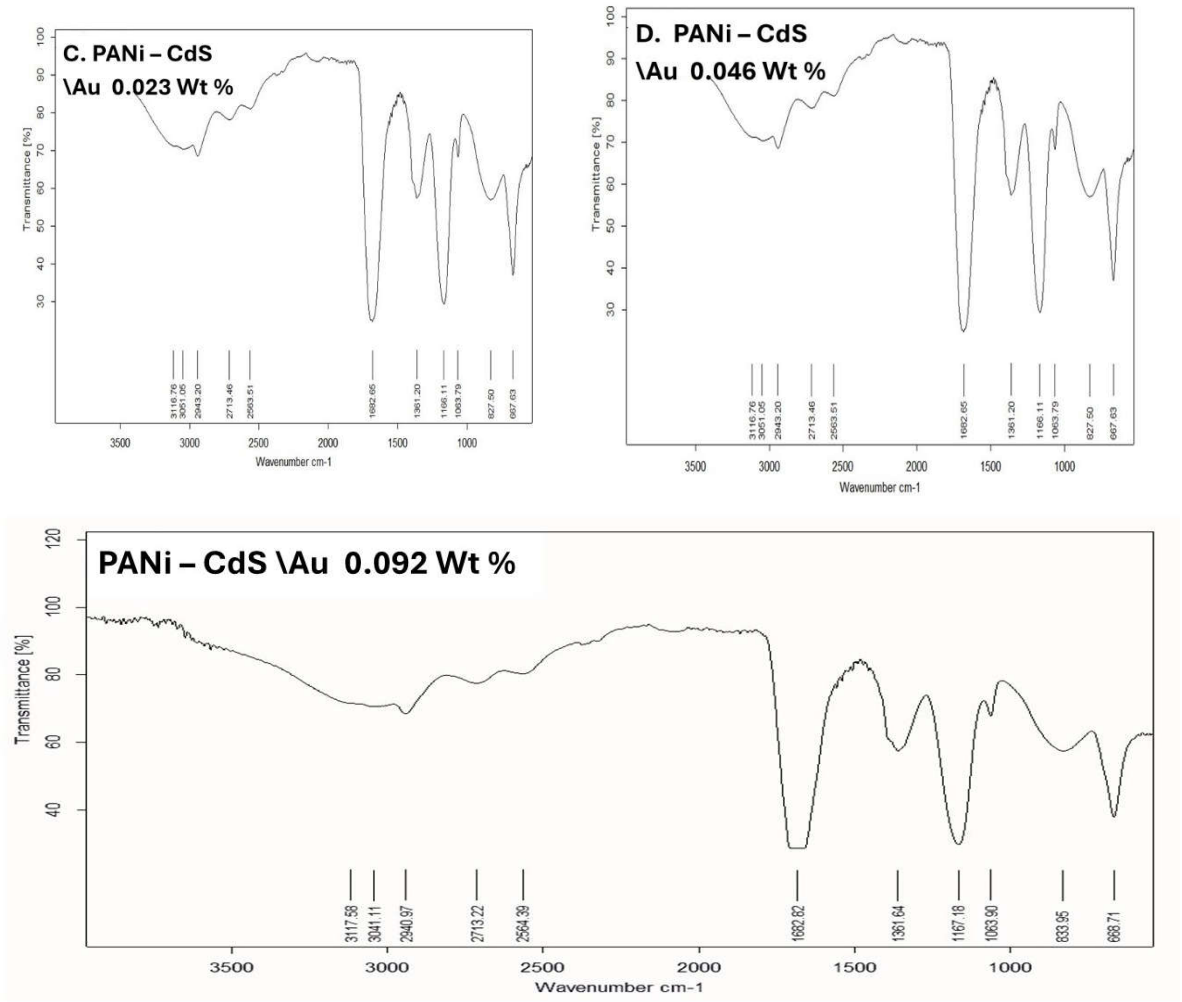

Figure 2. FTIR spectra of (A) pristine polyaniline (PANI), (B) cadmium sulfide (CdS) nanoparticles, and (C–E) PANI–CdS/Au nanocomposites containing Au at weight fractions of 0.023, 0.046, and 0.092, respectively.

In the PANI–CdS/Au nanocomposites (0.023, 0.046, and 0.092 wt% Au), gold itself does not contribute intrinsic IR-active modes. However, the spectra display organic absorptions such as a C=O stretching band near 1622–1692 cm^{-1}, suggesting the presence of stabilizing organic moieties on the nanoparticle surface. The characteristic PANI bands remain conserved, though slight shifts in peak positions and intensities are observed. These spectral modifications indicate electronic and interfacial interactions between PANI, CdS, and Au, consistent with the formation of a ternary nanocomposite system. The preservation of PANI's emeraldine features alongside Cd–S and surface-bound organic absorptions confirms successful integration of CdS and Au within the polymer matrix, while the subtle spectral changes highlight synergistic interactions that may enhance charge transfer and stability.

3.3. Structural Analysis of PANI, CdS and PANi-CdS/Au Nanocomposites

The The X-ray diffraction (XRD) patterns of pristine PANI, CdS nanoparticles, Au nanoparticles, and PANI–CdS/Au nanocomposites are presented. Pristine PANI exhibits a broad diffraction band centered at $2\theta \approx 25°$, which corresponds to the periodicity parallel to the polymer chains, confirming its semi-crystalline emeraldine base structure [34].

The XRD profile of CdS nanoparticles reveals a polycrystalline hexagonal wurtzite phase, with diffraction peaks at 2θ values of ~25.0°, 26.5°, 28.0°, 43.8°, 47.8°, and 51.9°, indexed to the (100), (002), (101), (110), (103), and (112) planes, respectively, in agreement with JCPDS card No. 23-0677 [35].

 doi:10.20944/preprints202602.1192.v1

The diffraction pattern of Au nanoparticles displays peaks at 2θ values of 37.2°, 43.4°, 63.6°, and 76.6°, corresponding to the (111), (200), (220), and (311) planes of the face-centered cubic (fcc) structure, consistent with JCPDS card No. 89-3697 [36].

In the PANI–CdS/Au nanocomposites, sharp and well-defined peaks are observed at 2θ ≈ 38.2°, 44.4°, and 77.3°, corresponding to the (111), (200), and (311) planes of Au nanoparticles. CdS retains its most intense peak at 2θ ≈ 28.9° (101 plane), while peaks at ~25.9° and ~26.7° overlap with the broad PANI band, producing a shoulder-like feature. The embedded Au nanoparticles preserve their cubic structure, while systematic rightward shifts in the (111) diffraction peak are observed across all composites, indicating contraction of interfacial spacing due to strong interactions between PANI chains and CdS/Au surfaces.

At higher Au loading (0.096 wt%), the diffraction peaks become sharper and more intense, suggesting reduced lattice defects and enhanced crystallinity. The lattice constant for Au nanoparticles in the (111) plane was calculated as a = b = c = 4.185 Å. In the PANI–CdS/Au nanocomposites, the lattice constant decreased to 4.060 Å at 0.023 wt% and slightly increased to 4.096 Å at 0.096 wt%, reflecting subtle strain relaxation.

Crystallite sizes were estimated using the Scherrer equation. For Au nanoparticles, the average crystallite size in the (111) plane was ~21.6 nm. In the PANI–CdS/Au nanocomposites, crystallite sizes decreased progressively with increasing Au content: 29 nm (0.023 wt%), 17.4 nm (0.046 wt%), and 15 nm (0.096 wt%). Dislocation density, calculated using equation (2), was 2.14 × 10^{15} for Au nanoparticles and increased with higher Au loading in the composites (1.19, 3.31, and 4.44 × 10^{15}), confirming the inverse relationship between crystallite size and dislocation density [38]. Microstrain, determined using equation (3), was 0.0016 for Au nanoparticles, with lower values observed in the nanocomposites (Table 1).

The observed peak broadening in the ternary composites is attributed not only to nanoscale effects but also to microstrain arising from mismatches in thermal expansion and lattice parameters among the metallic, semiconducting, and polymeric phases. These findings confirm successful integration of CdS and Au within the PANI matrix, with interfacial interactions enhancing crystallinity and potentially improving charge transport properties.

Table 1. The Crystallite Size, Lattice constant, Dislocation Density, Fine Strain Strain, Au NPS and PANI-CdS/Au Nanocomposites for (111) Plane.

Material	Crystallit Size (nm)	**a=b=c (A^0)**	**δ** line/m^2x10^{15}	Staring
Au NPS	21.6	4.185	2.143	0.0016046
PANI-CdS \Au (0.023)	29	4.060	1.189	0.002305
PANI–CdS\Au (0.046)	17.39	4.087	3.306	0.0047803
PANI–CdS\Au (0.092)	15	4.096	4.444	0.007970

$$\mathbf{D_{av}} = \frac{k\lambda}{\beta cos\theta} \quad \text{----------} \quad \mathbf{(1)}$$

$$\delta = \frac{1}{D_{av}^{\,2}} \quad \text{----------} \quad \mathbf{(2)}$$

$$\mathbf{Micro\text{-}Strain} = \frac{(d_{XRD} - d_{JCPDS})}{d_{JCPDS}} \quad \text{----------} \quad \mathbf{(3)}$$

$$d_{hkl} = \frac{a}{\sqrt{h^2+k^2+l^2}} \quad \text{----------} \quad \mathbf{(4)}$$

 doi:10.20944/preprints202602.1192.v1

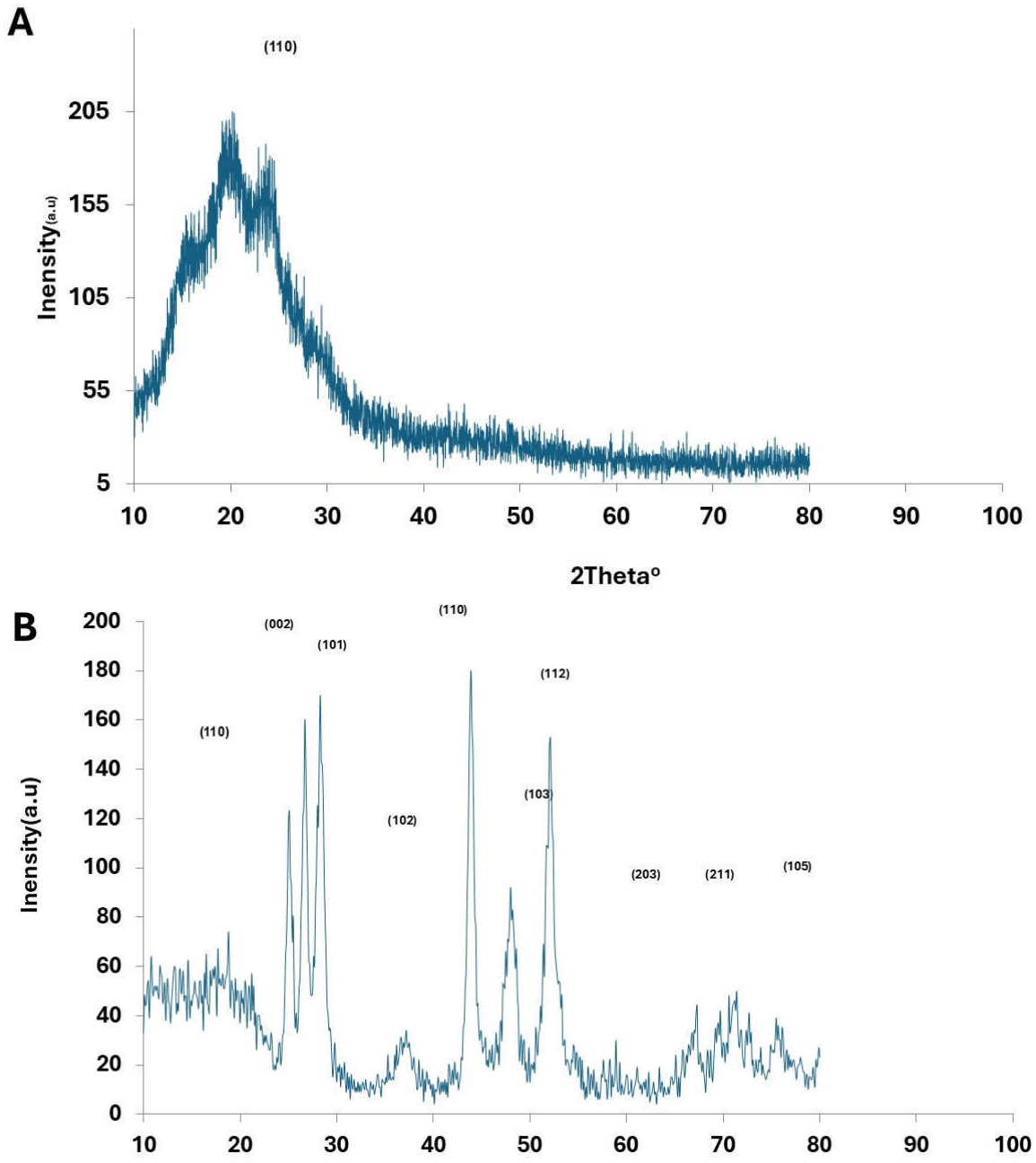

 doi:10.20944/preprints202602.1192.v1

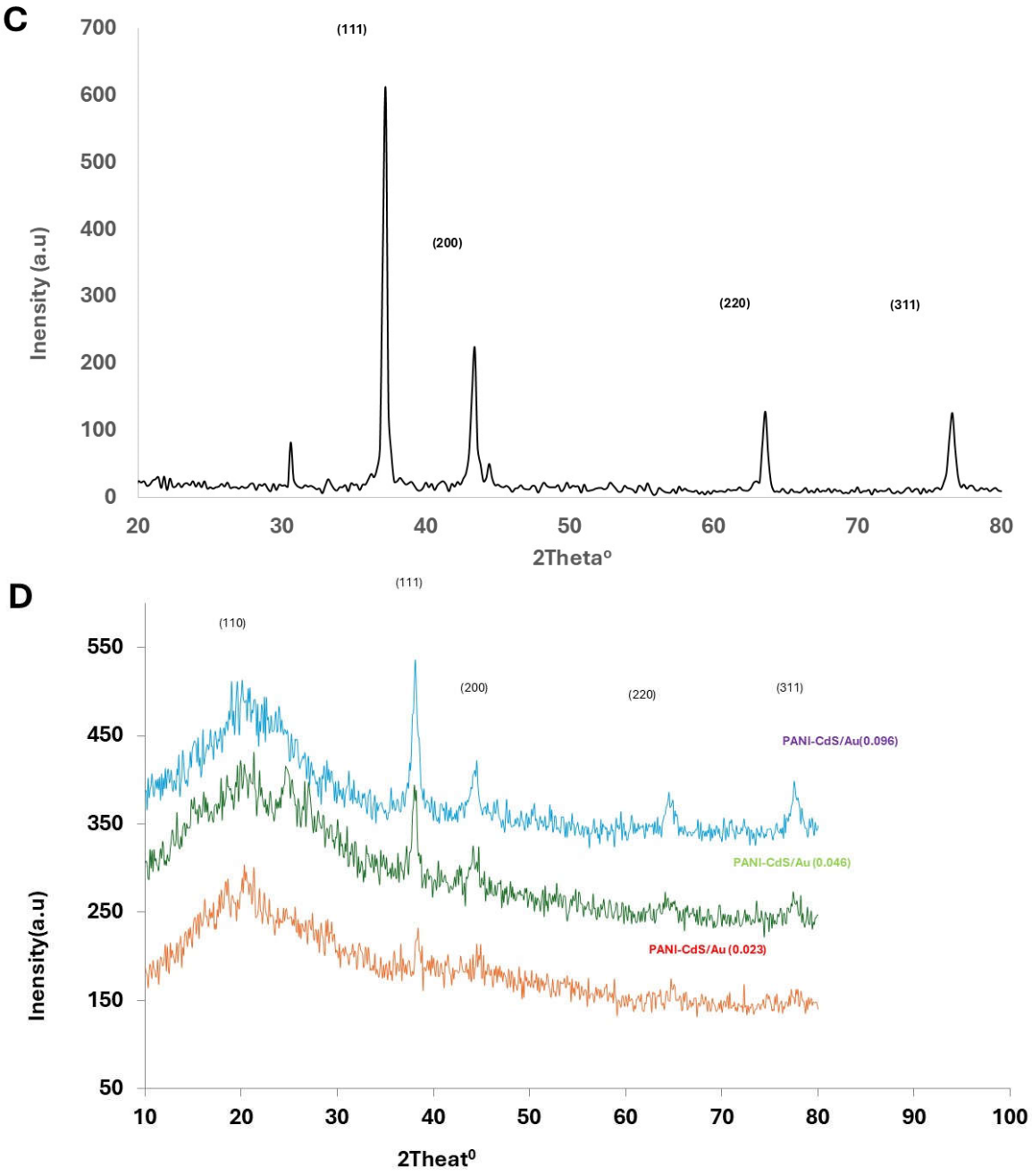

Figure 3. X-ray diffraction (XRD) patterns of (A) pristine polyaniline (PANI), (B) cadmium sulfide (CdS) nanoparticles, (C) gold nanoparticles (Au), and (D) PANI–CdS/Au nanocomposites containing Au at weight fractions of 0.023, 0.046, and 0.096, respectively.

3.4. Morphological Analysis

Field emission scanning electron microscopy (FESEM) images provide detailed insight into the morphology of Au nanoparticles and their incorporation within the PANI–CdS matrix. Pure Au nanoparticles (Figure 4A) exhibit a uniform spherical morphology with particle sizes ranging between ~27 and ~64 nm, consistent with nanoscale metallic Au. The absence of significant agglomeration confirms their colloidal stability and suitability for integration into hybrid nanostructures [39].

In the PANI–CdS/Au nanocomposites (Figure 4B–D), Au nanoparticles are uniformly distributed and strongly embedded within the polymer–semiconductor framework. At lower Au loading (0.023 wt%), the nanoparticles appear sparsely dispersed, with partial embedding in the PANI–CdS matrix, suggesting initial nucleation and stabilization by the polymer chains. At intermediate loading (0.046 wt%), the distribution becomes denser, with Au nanoparticles forming

 doi:10.20944/preprints202602.1192.v1

intimate contact with CdS domains, indicative of enhanced interfacial interactions. At higher loading (0.092 wt%), the nanoparticles are more abundant and uniformly dispersed, with minimal agglomeration, reflecting effective stabilization by the PANI matrix.

This progressive improvement in nanoparticle dispersion and interfacial adhesion is critical for functional performance. The high surface-to-volume ratio maintained even at elevated Au content maximizes effective contact between the nanocomposite and external environments, which is particularly relevant for antimicrobial activity. The morphological evidence corroborates the XRD and FTIR findings, confirming successful integration of Au nanoparticles into the PANI–CdS framework and highlighting synergistic structural interactions that enhance charge transfer, stability, and bioactivity [40].

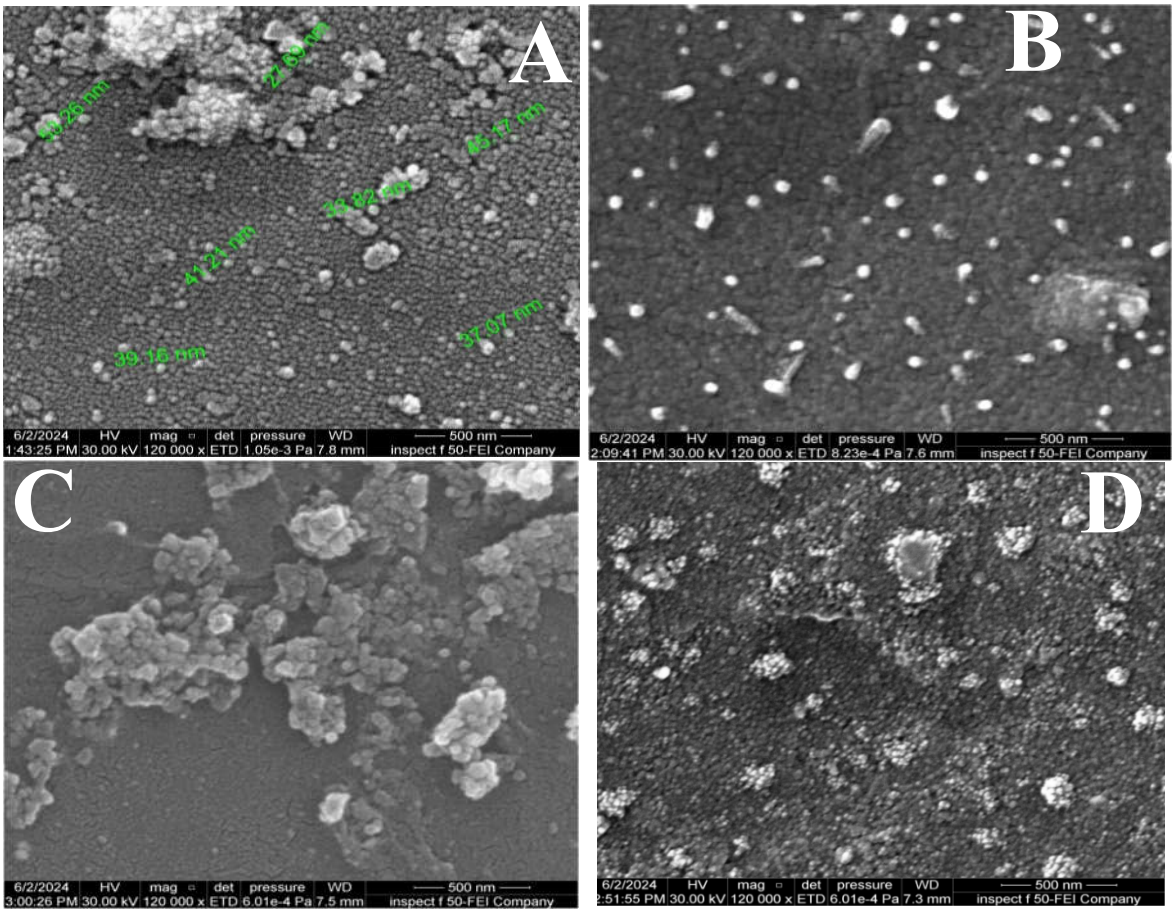

Figure 4. FESEM micrographs of (A) Au nanoparticles and (B–D) PANI–CdS/Au nanocomposites containing Au at weight fractions of 0.023, 0.046, and 0.092, respectively.

3.5. Antibacterial Activity of PANi-CdS/Au Nanocomposites

The The antibacterial performance of PANI–CdS/Au nanocomposites with varying Au nanoparticle loadings (0.023, 0.046, and 0.092 wt%) was assessed using the agar well diffusion method against Staphylococcus aureus (Gram-positive) and Escherichia coli (Gram-negative). Clear inhibition zones were observed around the discs, confirming effective bactericidal activity. The nanocomposites demonstrated stronger inhibitory effects against E. coli, which can be attributed to its thinner and more permeable cell wall compared to the thicker peptidoglycan layer of S. aureus.

The enhanced antibacterial activity is consistent with the synergistic electronic interactions among PANI, CdS, and Au, as indicated by UV–Vis redshift analysis. This synergy facilitates the generation of reactive oxygen species (ROS), which are primarily responsible for bacterial cell damage. The spatial distribution of Au nanoparticles within the composite ensures that ROS are generated in close proximity to bacterial membranes, thereby increasing their destructive efficiency [41,42].

 doi:10.20944/preprints202602.1192.v1

The antibacterial mechanism involves direct nanoparticle–cell wall interactions, leading to encapsulation, rupture, and cytoplasmic leakage. Nanoparticles adhere to bacterial surfaces, impairing permeability and disrupting membrane integrity. In addition, polyaniline contributes intrinsic antibacterial properties through multiple mechanisms: surface hydrophilicity [43], extended polymer chain length [44], low molar mass [45], electrostatic attraction between positively charged PANI and negatively charged bacterial surfaces [46], and the presence of amino groups that enhance binding interactions [47,48].

Overall, the FESEM, XRD, and FTIR findings corroborate the antimicrobial assay results, confirming that the structural integration of Au nanoparticles within the PANI–CdS matrix enhances stability, charge transfer, and bactericidal efficiency. The observed dose-dependent inhibition zones highlight the potential of these nanocomposites for biomedical and antimicrobial applications.

Table 2. The Crystallite Size, Lattice constant, Dislocation Density, Fine Strain Strain, Au NPS and PANI-CdS/Au Nanocomposites for (111) Plane.

Bacteria	Concentration of ($100\mu g/ml$) (PANI/CdS-Au)Wt% inhibition zone (mm)		
	PANI/CdS-Au(0.023)Wt%	PANI/CdS-Au(0.046) Wt%	PANI/CdS-Au(0.092)Wt%
Staph. ureus	20	22	24
E. coli	23	27	36
Staph. ureus	15	16	18
E. coli	17	18	20

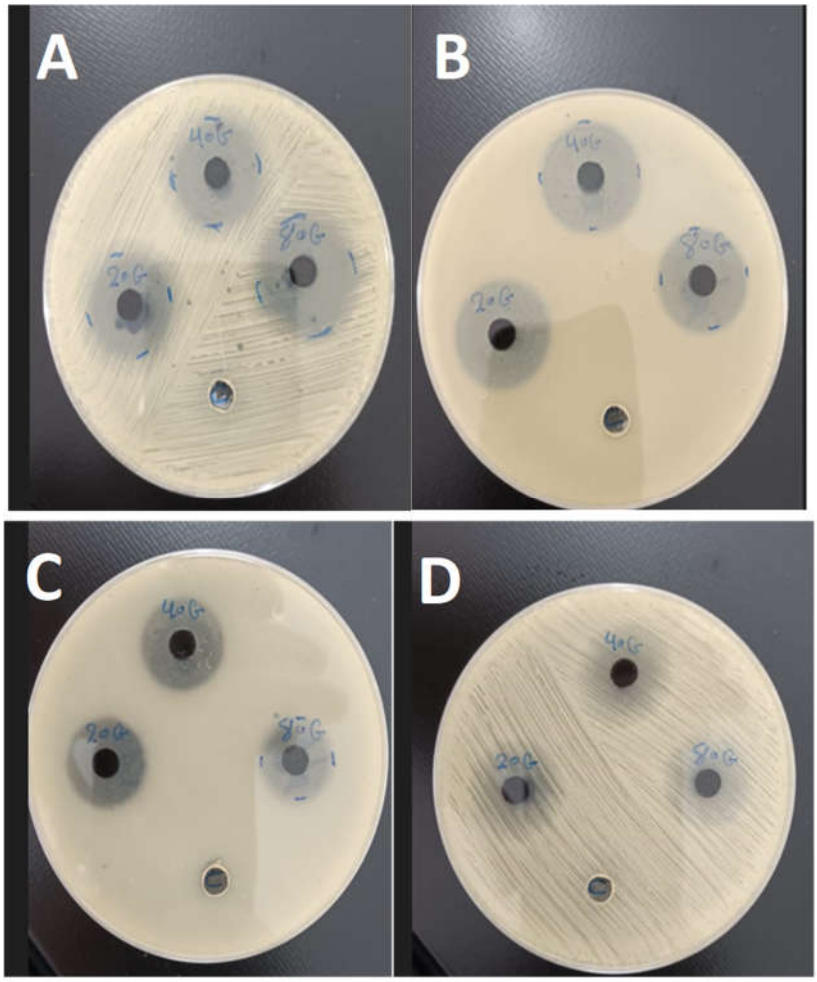

Figure 5. Antibacterial activity of PANI–CdS/Au nanocomposites containing Au at weight fractions of 0.023, 0.046, and 0.092, evaluated by the agar diffusion method. Inhibition zones were measured at a concentration of

 doi:10.20944/preprints202602.1192.v1

100 µg/mL against (A) Staphylococcus aureus and (B) Escherichia coli, and at 25 µg/mL against (C) E. coli and (D) S. aureus.

4. Discussion

The structural, spectroscopic, and morphological analyses collectively confirm the successful integration of CdS and Au nanoparticles within the PANI matrix. XRD results revealed distinct diffraction peaks corresponding to Au and CdS phases, with noticeable shifts in the (111) plane of Au, indicating lattice contraction and strong interfacial interactions between the metallic nanoparticles and the polymer backbone [27,28,35]. This observation was further supported by FTIR spectra, which showed conserved PANI vibrational bands with slight intensity variations, consistent with electronic coupling among PANI, CdS, and Au [33,34].

UV–Vis absorption spectra demonstrated a pronounced redshift at higher Au loading (0.092 wt%), suggesting enhanced electron delocalization and improved light-harvesting capability. This redshift implies that the nanocomposite can absorb lower-energy photons, facilitating efficient electron excitation and charge transfer [37,38]. The FE-SEM micrographs confirmed a uniform distribution of spherical Au nanoparticles within the PANI–CdS matrix, with no evidence of agglomeration even at the highest loading. The resulting high surface-to-volume ratio is critical for maximizing interfacial contact with bacterial membranes [39,40].

The antimicrobial assays revealed superior activity against Escherichia coli compared to Staphylococcus aureus, which can be attributed to differences in cell wall structure [41,42]. The synergy between PANI, CdS, and Au enhances the generation of reactive oxygen species (ROS), which disrupt bacterial membranes and cytoplasmic integrity [9,10,19]. Gold nanoparticles act as catalytic centers, facilitating charge transfer and suppressing electron–hole recombination, thereby amplifying ROS production [11,36]. Polyaniline contributes additional antibacterial functionality through its hydrophilic surface, electrostatic interactions, and amino group chemistry [43–48].

At 0.092 wt% Au, the nanocomposite exhibited the highest antimicrobial efficiency, underscoring the importance of optimized nanoparticle loading. The combination of structural stability, efficient charge transfer, and enhanced ROS generation positions PANI–CdS/Au nanocomposites as promising candidates for applications in water sterilization, antibacterial coatings, and biomedical devices. This study highlights the synergistic integration of microbiology and nanotechnology, offering promising advances in the development of next-generation antibacterial formulations.

5. Conclusions

A variation in the lattice modulus of gold nanoparticles within the PANI–CdS/Au nanocomposite was observed, confirming interfacial interactions between Au nanoparticles and the PANI–CdS matrix. FTIR spectra demonstrated that the characteristic PANI bands were preserved, with slight intensity shifts indicative of electronic coupling among PANI, CdS, and Au. UV–Vis absorption analysis further revealed that at 0.092 wt% Au, a pronounced redshift occurred, signifying enhanced absorption of lower-energy (longer-wavelength) photons capable of activating electron transitions.

Morphological examination confirmed the absence of agglomeration even at the highest Au loading (0.092 wt%), thereby maintaining a high surface-to-volume ratio. This structural feature is critical for maximizing antimicrobial interactions with bacterial membranes. Gold nanoparticles act as catalytic centers, facilitating charge transfer and suppressing electron–hole recombination, which enhances the efficiency of ROS generation. These reactive species contribute to membrane disruption and cytoplasmic damage, ultimately leading to bacterial cell death.

At 0.092 wt% Au, the nanocomposite exhibited the highest antimicrobial activity, underscoring its potential as a candidate material for water sterilization and antibacterial medical coatings. This

 doi:10.20944/preprints202602.1192.v1

study highlights the synergistic integration of microbiology and nanotechnology, offering promising advances in the development of next-generation antibacterial formulations.

6. Patents

Not applicable.

Supplementary Materials: No supplementary data.

Author Contributions: Conceptualization was carried out by Raad Al-Kilabi and Abdulameer H. Ali. Methodology was designed by Hude Al-Allaq and Elias F. Muhammed. Validation was conducted by Raad Al-Kilabi, Sahib Alkulaibi, and Adel Alkhayatt. Formal analysis was undertaken by Haider Al-Hello, Abdulameer H. Ali. Investigation was performed by Hude Al-Allaq and Elias F. Muhammed. Resources were provided by Sahib Alkulaibi. Data curation was managed by Elias F. Muhammed and Haider Al-Hello. Writing—original draft preparation was completed by Raad Al-Kilabi and Abdulameer H. Ali. Writing—review and editing was handled by Adel Alkhayatt and Haider Al-Hello. Visualization was prepared by Elias F. Muhammed. Supervision was provided by Haider Al-Hello. Project administration was overseen by Haider Al-Hello. Funding acquisition was secured by Haider Al-Hello. All authors have read and agreed to the published version of the manuscript.

Funding: Please add: This research received no external funding.

Conflicts of Interest: The authors declare no conflicts of interest.

 doi:10.20944/preprints202602.1192.v1

References

1. David, W.H.; Mira, J. Composites of intrinsically conducting polymers as sensing nanomaterials. Chem. Rev. 2008, 108, 746–769.
2. Ma, X.; Li, G.; Wang, M.; Cheng, Y.; Bai, R.; Chen, H. Preparation of nano-wire structured polyaniline composite and its gas-sensitivity studies. Chem. Eur. J. 2006, 12, 3254–3260.
3. Ma, X.; Li, G.; Wang, M.; Bai, R.; Yang, F.; Chen, H. Unusual electrical response of poly(aniline) composite film on exposure to the atmosphere of base and its applications on sensors. Green Chem. 2006, 8, 63–69.
4. Huang, J.; Virji, S.; Weiller, B.H.; Kaner, R.B. Nanostructured polyaniline sensors. Chem. Eur. J. 2004, 10, 1314–1319.
5. Huang, J.; Kaner, R.B. Nanofiber formation in the chemical polymerization of aniline: A mechanistic study. Angew. Chem. Int. Ed. 2004, 43, 5817–5821.
6. Xu, S.; Gao, T.; Feng, X.; Fan, X.; Liu, G.; Mao, Y.; Yu, X.; Lin, J.; Luo, X. Near infrared fluorescent dual ligand functionalized Au NCs based multidimensional sensor array for pattern recognition of multiple proteins and serum discrimination. Biosens. Bioelectron. 2017, 97, 203–207.
7. Amoli-Diva, M.; Sadighi-Bonabi, R.; Pourghazi, K. Switchable on/off drug release from gold nanoparticles-grafted dual light- and temperature-responsive hydrogel for controlled drug delivery. Mater. Sci. Eng. C 2017, 76, 242–248.
8. Shukla, R. Studies on assessment of biocompatibility of gold and silver nanoparticles in cell culture for tissue engineering applications. Ph.D. Thesis, Shodhganga Repository, 2013. Available online: http://shodhganga.inflibnet.ac.in/handle/10603/2221 (shodhganga.inflibnet.ac.in in Bing) (accessed on 21 April 2013).
9. Jain, P.K.; Lee, K.S.; El-Sayed, I.H.; El-Sayed, M.A. Calculated absorption and scattering properties of gold nanoparticles of different size, shape, and composition: Applications in biological imaging and biomedicine. J. Phys. Chem. B 2006, 110, 7238–7248.
10. Huang, X.; Jain, P.K.; El-Sayed, I.H.; El-Sayed, M.A. Gold nanoparticles: Interesting optical properties and recent applications in cancer diagnostics and therapy. Nanomedicine 2007, 2, 681–693.
11. Burda, C.; Chen, X.; Narayanan, R.; El-Sayed, M.A. Chemistry and properties of nanocrystals of different shapes. Chem. Rev. 2005, 105, 1025–1102.
12. Lipka, J.; Semmler-Behnke, M.; Sperling, R.A.; Wenk, A.; Takenaka, S.; Schleh, C.; Kissel, T.; Parak, W.J.; Kreyling, W.G. Biodistribution of PEG-modified gold nanoparticles following intratracheal instillation and intravenous injection. Biomaterials 2010, 31, 6574–6581.
13. Sharma, A.; Matharu, Z.; Sumana, G.; Solanki, P.R.; Kim, C.G.; Malhotra, B.D. Antibody immobilized cysteamine functionalized-gold nanoparticles for aflatoxin detection. Thin Solid Films 2010, 519, 1213–1218.
14. Zheng, J.Z.; Tang, R.; Chen, Y.; Miranda, O.; Rotello, V.M.; Vachet, W. Determination of the intracellular stability of gold nanoparticle monolayers using mass spectrometry. Anal. Chem. 2012, 84, 4321–4326.
15. Cho, E.C.; Zhang, Q.; Xia, Y. The effect of sedimentation and diffusion on cellular uptake of gold nanoparticles. Nat. Nanotechnol. 2011, 6, 385–391.
16. Badwaik, V.D.; Bartonojo, J.; Evans, J.; Sahi, S.; Willis, C.; Rajalingam, D. Single-step biofriendly synthesis of surface modifiable near-spherical gold nanoparticles for applications in biological detection and catalysis. Langmuir 2011, 27, 5549–5554.
17. Peana, M.; Pelucelli, A.; Chasapis, C.T.; Perlepes, S.P.; Bekiari, V.; Medici, S.; Zoroddu, M.A. Biological effects of human exposure to environmental cadmium. Biomolecules 2023, 13, 36.
18. Suhani, I.; Sahab, S.; Srivastava, V.; Singh, R.P. Impact of cadmium pollution on food safety and human health. Curr. Opin. Toxicol. 2021, 27, 1–7.
19. Huang, M.; Liu, C.; Cui, P.; Wu, T.; Feng, X.; Huang, H.; Zhou, J.; Wang, Y. Facet-dependent photoinduced transformation of cadmium sulfide (CdS) nanoparticles. Environ. Sci. Technol. 2021, 55, 13132–13141.
20. Wu, Q.; Huang, L.; Li, Z.; An, W.; Liu, D.; Lin, J.; Tian, L.; Wang, X.; Liu, B.; Qi, W.; et al. The potential application of raw cadmium sulfide nanoparticles as CT photographic developer. Nanoscale Res. Lett. 2016, 11, 232.

 doi:10.20944/preprints202602.1192.v1

21. Dabhane, H.; Ghotekar, S.; Tambade, P.; Pansambal, S.; Murthy, H.A.; Oza, R.; Medhane, V. A review on environmentally benevolent synthesis of CdS nanoparticles and their applications. Environ. Chem. Ecotoxicol. 2021, 3, 209–219.
22. Varmazyari, A.; Baris, O. Rapid biosynthesis of cadmium sulfide (CdS) nanoparticles using culture supernatants of Viridibacillus arenosi K64. BioNanoSci. 2022, 12, 191–202.
23. Shakibaie, M.; Riahi-Madvar, S.; Ameri, A.; Amiri-Moghadam, P.; Adeli-Sardou, M.; Forootanfar, H. Microwave-assisted biosynthesis of cadmium nanoparticles: Characterization, antioxidant and cytotoxicity studies. J. Clust. Sci. 2022, 33, 1877–1887.
24. Harish, R.; Nisha, K.D.; Prabakaran, S.; Sridevi, B.; Harish, S.; Navaneethan, M.; Ponnusamy, S.; Hayakawa, Y.; Vinniee, C.; Ganesh, M.R. Cytotoxicity assessment of chitosan-coated CdS nanoparticles for bio-imaging applications. Appl. Surf. Sci. 2020, 499, 143817.
25. Skirtach, A.G.; Dejugnat, C.; Braun, D.; Susha, A.S.; Rogach, A.L.; Parak, W.J.; Möhwald, H.; Sukhorukov, G.B. Nanoengineered polyelectrolyte capsules for intracellular delivery. Nano Lett. 2005, 5, 1371–1377.
26. Jose, A.; Bansal, M.; Svirskis, D.; Swift, S.; Gizdavic-Nikolaidis, M.R. Synthesis and characterization of antimicrobial colloidal polyanilines. Colloids Surf. B 2024, 238, 113912.
27. Un, B.; Vodnik, V.V.; Ahrenkiel, S.P.; Stoiljković, M.; Marjanović, G.C.; Nedeljković, J.M. Interfacial synthesis and characterization of gold/polyaniline nanocomposites. Synth. Met. 2014, 195, 122–131.
28. Khanna, P.K.; Sunil, P.L.; Subbarao, V.V.V.S.; Ki-Won, J. Polyaniline–CdS nanocomposite from organometallic cadmium precursor. Mater. Chem. Phys. 2004, 87, 49–52.
29. Thirunavukkarasu, K.K.; Saranya, B.; Janarthanan, J.; Chandrasekaran, J. Design, fabrication and working of in-house spin coating unit for thin deposition. Int. J. Innov. Res. Sci. Eng. Technol. 2016, 5, 6.
30. Obaid, M.N.; Hassan, S.M. A.C. electrical properties of pure and doped polyaniline salt prepared by electrochemical polymerization. Adv. Environ. Biol. 2017, 11, 2, 17–26.
31. Sánchez, J.D.; Rosas-Aburto, A.; Vivaldo-Lima, E.; Gimeno, M. Development and characterization of a flexible electrochromic device based on polyaniline and enzymatically synthesized poly(gallic acid). Synth. Met. 2017, 223, 43–48.
32. Arenas, M.C.; Andablo, E.; Castaño, V.M. Synthesis of conducting polyaniline nanofibers from single and binary dopant agents. J. Nanosci. Nanotechnol. 2010, 10, 549–554.
33. Trchová, M.; Stejskal, J. Polyaniline: The infrared spectroscopy of conducting polymer nanotubes. Pure Appl. Chem. 2011, 83, 1803–1817.
34. Hussein, R.; Omran, A.H.; Ressen, A.H. Preparation, characterization and antibacterial activity of polyaniline–CdS nanocomposites. J. Phys. Conf. Ser. 2021, 1999, 2nd International Virtual Conference on Pure Science (2IVCPS 2021), 21–22 April.
35. Hadi, I.H.; Khashan, K.S.; Sulaiman, D. Cadmium sulphide (CdS) nanoparticles: Preparation and characterization. Mater. Today Proc. 2021,.
36. Jamil, I.; Shamir, K.; Sajid, Q.; Iftikhar, R.; Maryam, E.; Rafaqat, R.; Bibi, R.; Saleem, I.; Nawab, A.; Mumtaz, S.; Wali, A.; Akitsu, T.; Ahmad, F. A review on the synthesis and fabrication of gold nanoparticles and their application in dyes degradation. Preprints 2024, doi:10.20944/preprints202402.1236.v1.
37. Ma, X.; Li, C.; Zhang, X.; Gao, M.; Li, G. Broadband spectrum light-driven PANI/Au/beta-cyclodextrin nanocomposite and its light-triggered interfacial carrier transfer. Coatings 2022, 12, 1401. https://doi.org/10.3390/coatings12101401 (doi.org in Bing)
38. J.I., C.; J.D.; A.F.; R.L.; M.E.A.; J.A.B. Structural and optical modifications of CdS properties in CdS–Au thin films prepared by CBD. Results Phys. 2021, doi:10.1016/j.rinp.2021.103914.
39. Platnich, C.M.; Banerjee, A.; Kollath, V.O.; Karan, K.; Trudel, S. Thiol-ene click microcontact printing of gold nanoparticles onto silicon surfaces. Can. J. Chem. 2018, 96, 190–195.
40. Hu, T.; Shan, S.; Yang, S.; Jiang, L.; Wang, Y.; Jia, Q. One-step synthesis and antibacterial properties of polyaniline/TiO_2 nanocomposites. Adv. Mater. Res. 2012, 534, 78–81.
41. Panáček, A.; Kvitek, L.; Prucek, R.; Kolář, M.; Večeřová, R.; Pizúrová, N.; Sharma, V.K.; Nevěčná, T.; Zbořil, R. Silver colloid nanoparticles: Synthesis, characterization, and their antibacterial activity. J. Phys. Chem. B 2006, 110, 16248–16253.

 doi:10.20944/preprints202602.1192.v1

42. Honary, S.; Ghajar, K.; Khazaeli, P.; Shalchian, P. Preparation, characterization, and antibacterial properties of silver–chitosan nanocomposites using different molecular weight grades of chitosan. Trop. J. Pharm. Res. 2011, 10, 69–74.
43. Prabhakar, P.K.; Raj, S.; Anuradha, P.R.; Sawant, S.N.; Doble, M. Biocompatibility studies on polyaniline and polyaniline–silver nanoparticle coated polyurethane composite. Colloids Surf. B 2011, 86, 146–153.
44. Nikolaidis, M.R.G.; Bennett, J.; Zujovic, Z.; Swift, S.; Bowmaker, G.A. Characterization and antimicrobial efficacy of acetone-extracted aniline oligomers. Synth. Met. 2012, 162, 1114–1119.
45. Humpolíček, P.; Kašpárková, V.; Saha, P.; Stejskal, J. Biocompatibility of polyaniline. Synth. Met. 2012, 162, 722–727.
46. Zuo, H.; Wu, D.; Fu, R. Preparation of antibacterial poly(methyl methacrylate) by solution blending with water-insoluble antibacterial agent poly[(tert-butylamino)ethyl methacrylate]. J. Appl. Polym. Sci. 2012, 125, 3537–3544.
47. Wu, C.S. Preparation and characterization of an aromatic polyester/polyaniline composite and its improved counterpart. Polym. Lett. 2012, 6, 465–475.
48. Wu, C.S. Aliphatic–aromatic polyester–polyaniline composites: Preparation, characterization, antibacterial activity and conducting properties. Polym. Int. 2012, 61, 1556–1563.